As I will illustrate in later chapters, the crucial part of data regularization problems is in the choice and implementation of the regularization operator **D** or the corresponding preconditioning operator **P**. The choice of the forward modeling operator **L** is less critical. In this chapter, I discuss the nature of forward interpolation, which has been one of the traditional subjects in computational mathematics. Wolberg (1990) presents a detailed review of different conventional approaches. I discuss a simple mathematical theory of interpolation from a regular grid and derive the main formulas from a very general idea of function bases.

Forward interpolation plays only a supplementary role in this dissertation, but it has many primary applications, such as trace resampling, NMO, Kirchhoff and Stolt migrations, log-stretch, and radial transform, in seismic data processing and imaging. Two simple examples appear at the end of this chapter.

INTERPOLATION THEORY

Mathematical interpolation theory considers a function f, defined on a regular grid N. The problem is to find f in a continuum that includes N. I am not defining the dimensionality of N and f here because it is not essential for the derivations. Furthermore, I am not specifying the exact meaning of "regular grid," since it will become clear from the analysis that follows. The function f is assumed to belong to a Hilbert space with a defined dot product.

If we restrict our consideration to a linear case, the desired solution will take the following general form

$$f(x) = \sum_{n \in N} W(x,n) f(n) \ , \tag{1}$$

where x is a point from the continuum, and $W(x,n)$ is a linear weight function that can take both positive and negative values. If the grid N itself is considered as continuous, the sum in formula (1) transforms to an integral in dn. Two general properties of the linear weighting function $W(x,n)$ are evident from formula (1).

Property 1

$$W(n,n) = 1 \ . \tag{2}$$

Equality (2) is necessary to assure that the interpolation of a single spike at some point n does not change the value $f(n)$ at the spike.

Property 2

$$\sum_{n \in N} W(x,n) = 1 \ . \tag{3}$$

This property is the normalization condition. Formula (3) assures that interpolation of a constant function $f(n)$ remains constant.

One classic example of the interpolation weight $W(x,n)$ is the Lagrange polynomial, which has the form

$$W(x,n) = \prod_{i \neq n} \frac{(x-i)}{(n-i)} \; . \tag{4}$$

The Lagrange interpolation provides a unique polynomial, which goes exactly through the data points $f(n)$[1]. The local 1-point Lagrange interpolation is equivalent to the nearest-neighbor interpolation, defined by the formula

$$W(x,n) = \begin{cases} 1, & \text{for} \quad n-1/2 \leq x < n+1/2 \\ 0, & \text{otherwise} \end{cases} \tag{5}$$

Likewise, the local 2-point Lagrange interpolation is equivalent to the linear interpolation, defined by the formula

$$W(x,n) = \begin{cases} 1-|x-n|, & \text{for} \quad n-1 \leq x < n+1 \\ 0, & \text{otherwise} \end{cases} \tag{6}$$

Because of their simplicity, the nearest-neighbor and linear interpolation methods are very practical and easy to apply. Their accuracy is, however, limited and may be inadequate for interpolating high-frequency signals. The shapes of interpolants (5) and (6) and their spectra are plotted in Figures 1 and 2. The spectral plots show that both interpolants act as low-pass filters, preventing the high-frequency energy from being correctly interpolated.

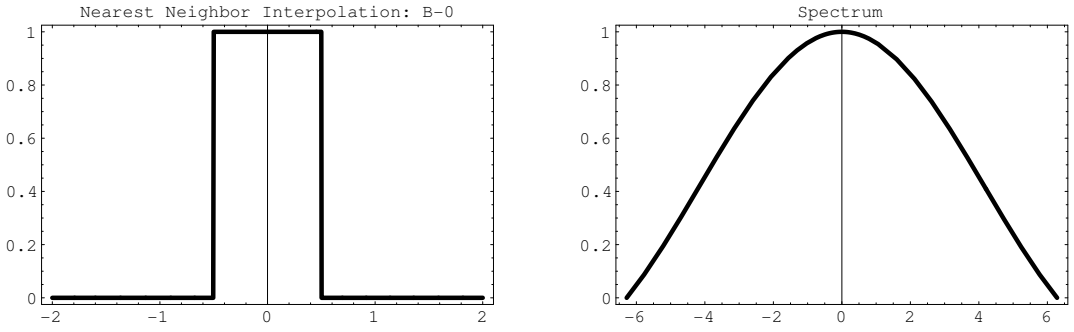

Figure 1: Nearest-neighbor interpolant (left) and its spectrum (right).

The Lagrange interpolants of higher order correspond to more complicated polynomials. Another popular practical approach is cubic convolution (Keys, 1981). The cubic convolution interpolant is a local piece-wise cubic function:

$$W(x,n) = \begin{cases} 3/2|x-n|^3 - 5/2|x-n|^2 + 1, & \text{for} \quad 0 \leq |x-n| < 1 \\ -1/2|x-n|^3 + 5/2|x-n|^2 - 4|x-n| + 2, & \text{for} \quad 1 \leq |x-n| < 2 \\ 0, & \text{otherwise} \end{cases} \tag{7}$$

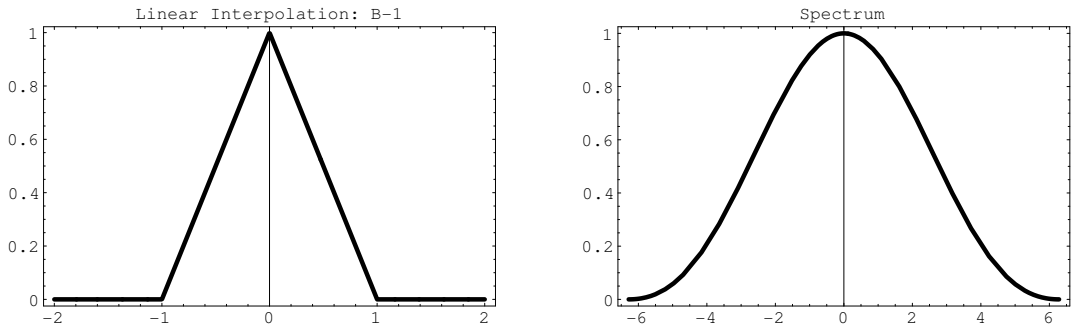

Figure 2: Linear interpolant (left) and its spectrum (right).

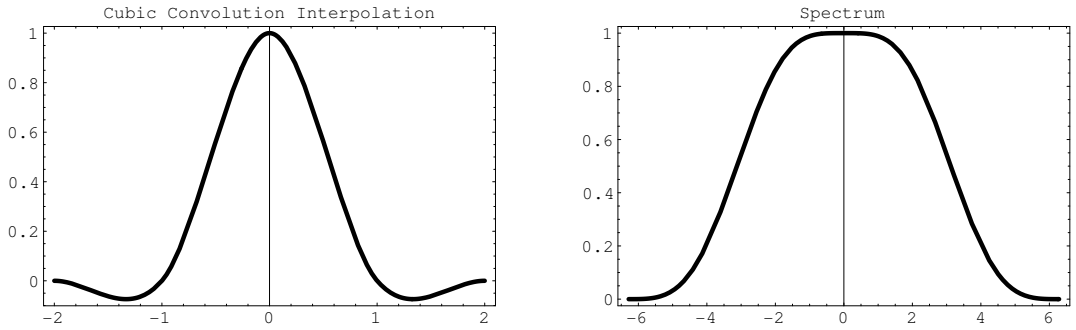

Figure 3: Cubic-convolution interpolant (left) and its spectrum (right).

The shapes of interpolant (7) and its spectrum are plotted in Figure 3.

I compare the accuracy of different forward interpolation methods on a one-dimensional signal shown in Figure 4. The ideal signal has an exponential amplitude decay and a quadratic frequency increase from the center towards the edges. It is sampled at a regular 50-point grid and interpolated to 500 regularly sampled locations. The interpolation result is compared with the ideal one. Figures 5 and 6 show the interpolation error steadily decreasing as we proceed from 1-point nearest-neighbor to 2-point linear and 4-point cubic-convolution interpolation. At the same time, the cost of interpolation grows proportionally to the interpolant length.

FUNCTION BASIS

A particular form of the solution (1) arises from assuming the existence of a basis function set $\{\psi_k(x)\},\ k \in K$, such that the function $f(x)$ can be represented by a

[1]It is interesting to note that the interpolation and finite-difference filters developed by Karrenbach (1995) from a general approach of self-similar operators reduce to a localized form of Lagrange polynomials.

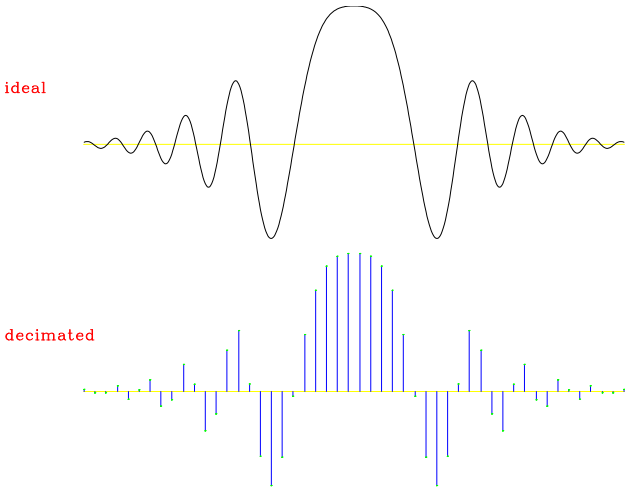

Figure 4: One-dimensional test signal. Top: ideal. Bottom: sampled at 50 regularly spaced points. The bottom plot is the input in a forward interpolation test.

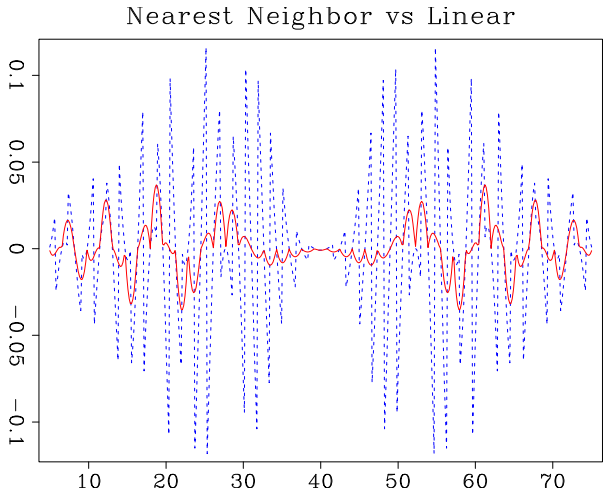

Figure 5: Interpolation error of the nearest-neighbor interpolant (dashed line) compared to that of the linear interpolant (solid line).

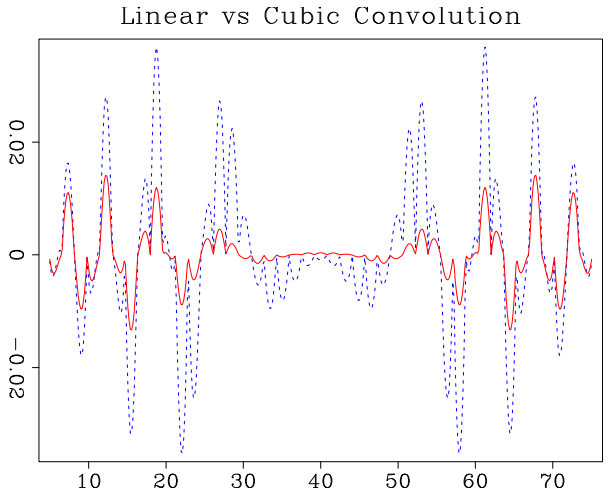

Figure 6: Interpolation error of the linear interpolant (dashed line) compared to that of the cubic convolution interpolant (solid line).

linear combination of the basis functions in the set, as follows:

$$f(x) = \sum_{k \in K} c_k \psi_k(x) \ . \tag{8}$$

We can find the linear coefficients c_k by multiplying both sides of equation (8) by one of the basis functions (e.g. $\psi_j(x)$). Inverting the equality

$$(\psi_j(x), f(x)) = \sum_{k \in K} c_k \Psi_{jk} \ , \tag{9}$$

where the parentheses denote the dot product, and

$$\Psi_{jk} = (\psi_j(x), \psi_k(x)) \ , \tag{10}$$

leads to the following explicit expression for the coefficients c_k:

$$c_k = \sum_{j \in K} \Psi^{-1}_{kj} \left(\psi_j(x), f(x)\right) \ . \tag{11}$$

Here Ψ^{-1}_{kj} refers to the kj component of the matrix, which is the inverse of Ψ. The matrix Ψ is invertible as long as the basis set of functions is linearly independent. In the special case of an orthonormal basis, Ψ reduces to the identity matrix:

$$\Psi_{jk} = \Psi^{-1}_{kj} = \delta_{jk} \ . \tag{12}$$

Equation (11) is a least-squares estimate of the coefficients c_k: one can alternatively derive it by minimizing the least-squares norm of the difference between $f(x)$ and the linear decomposition (8). For a given set of basis functions, equation (11) approximates the function $f(x)$ in formula (1) in the least-squares sense.

SOLUTION

The usual (although not unique) mathematical definition of the continuous dot product is

$$(f_1, f_2) = \int \bar{f}_1(x) f_2(x) dx \ , \tag{13}$$

where the bar over f_1 stands for complex conjugate (in the case of complex-valued functions). Applying definition (13) to the dot product in equation (11) and approximating the integral by a finite sum on the regular grid N, we arrive at the approximate equality

$$(\psi_j(x), f(x)) = \int \bar{\psi}_j(x) f(x) dx \approx \sum_{n \in N} \bar{\psi}_j(n) f(n) \ . \tag{14}$$

We can consider equation (14) not only as a useful approximation, but also as an implicit *definition* of the regular grid. Grid regularity means that approximation (14) is possible. According to this definition, the more regular the grid is, the more accurate is the approximation.

Substituting equality (14) into equations (11) and (8) yields a solution to the interpolation problem. The solution takes the form of equation (1) with

$$W(x,n) = \sum_{k\in K} \sum_{j\in K} \Psi^{-1}_{kj} \psi_k(x) \bar{\psi}_j(n) \ . \tag{15}$$

We have found a constructive way of creating the linear interpolation operator from a specified set of basis functions.

It is important to note that the adjoint of the linear operator in formula (1) is the continuous dot product of the functions $W(x,n)$ and $f(x)$. This simple observation follows from the definition of the adjoint operator and the simple equality

$$\left(f_1(x), \sum_{n\in N} W(x,n) f_2(n) \right) = \sum_{n\in N} f_2(n) \left(f_1(x), W(x,n) \right) = \left(\left(W(x,n), f_1(x) \right), f_2(n) \right) \ . \tag{16}$$

In the final equality, we have assumed that the discrete dot product is defined by the sum

$$\left(f_1(n), f_2(n) \right) = \sum_{n\in N} \bar{f}_1(n) f_2(n) \ . \tag{17}$$

Applying the adjoint interpolation operator to the function f, defined with the help of formula (15), and employing formulas (8) and (11), we discover that

$$\left(W(x,n), f(x) \right) = \sum_{k\in K} \sum_{j\in K} \Psi^{-1}_{kj} \bar{\psi}_j(n) \left(\psi_k(x), f(x) \right) =$$
$$\sum_{j\in K} \bar{\psi}_j(n) \sum_{k\in K} \Psi^{-1}_{jk} \left(\psi_k(x), f(x) \right) = \sum_{j\in K} c_j \psi_j(n) = f(n) \ . \tag{18}$$

This remarkable result shows that although the forward linear interpolation is based on approximation (14), the adjoint interpolation produces an exact value of $f(n)$! The approximate nature of equation (15) reflects the fundamental difference between adjoint and inverse linear operators (Claerbout, 1992).

When adjoint interpolation is applied to a constant function $f(x) \equiv 1$, it is natural to require the constant output $f(n) = 1$. This requirement leads to yet another general property of the interpolation functions $W(x,n)$:

Property 3

$$\int W(x,n) dx = 1 \ . \tag{19}$$

The functional basis approach to interpolation is well developed in the sampling theory (Garcia, 2000). Some classic examples are discussed in the next section.

INTERPOLATION WITH FOURIER BASIS

To illustrate the general theory with familiar examples, I consider in this section the most famous example of an orthonormal function basis, the Fourier basis of trigonometric functions. What kind of linear interpolation does this basis lead to?

Continuous Fourier basis

For the continuous Fourier transform, the set of basis functions is defined by

$$\psi_\omega(x) = \frac{1}{\sqrt{2\pi}} e^{i\omega x} \ , \tag{20}$$

where ω is the continuous frequency. For a 1-point sampling interval, the frequency is limited by the Nyquist condition: $|\omega| \le \pi$. In this case, the interpolation function W can be computed from equation (15) to be

$$W(x,n) = \frac{1}{2\pi} \int_{-\pi}^{\pi} e^{i\omega(x-n)} d\omega = \frac{\sin\left[\pi(x-n)\right]}{\pi(x-n)} \ . \tag{21}$$

The shape of the interpolation function (21) and its spectrum are shown in Figure 7. The spectrum is identically equal to 1 in the Nyquist frequency band.

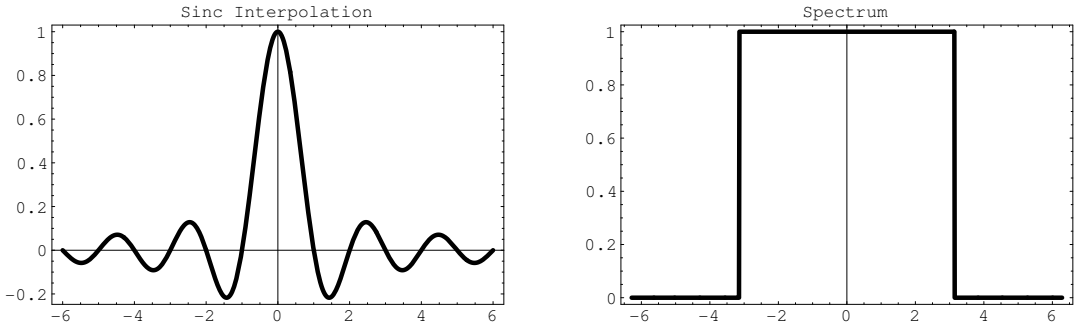

Figure 7: Sinc interpolant (left) and its spectrum (right).

Function (21) is well-known as the Shannon sinc interpolant. According to the sampling theorem (Kotel'nikov, 1933; Shannon, 1949), it provides an optimal interpolation for band-limited signals. A known problem prohibiting its practical implementation is the slow decay with $(x-n)$, which results in a far too expensive computation. This problem is solved in practice with heuristic tapering (Hale, 1980), such as triangle tapering (Harlan, 1982), or more sophisticated taper windows (Wolberg, 1990). One popular choice is the Kaiser window (Kaiser and Shafer, 1980), which has the form

$$W(x,n) = \begin{cases} \dfrac{\sin\left[\pi(x-n)\right]}{\pi(x-n)} \dfrac{I_0\left(a\sqrt{1-\left(\frac{x-n}{N}\right)^2}\right)}{I_0(a)} & \text{for} \qquad n-N < x < n+N \\ 0, & \text{otherwise} \end{cases} \tag{22}$$

where I_0 is the zero-order modified Bessel function of the first kind. The Kaiser-windowed sinc interpolant (22) has the adjustable parameter a, which controls the behavior of its spectrum. I have found empirically the value of $a = 4$ to provide a spectrum that deviates from 1 by no more than 1% in a relatively wide band.

While the function W from equation (21) automatically satisfies properties (3) and (19), where both x and n range from $-\infty$ to ∞, its tapered version may require additional normalization.

Figure 8 compares the interpolation error of the 8-point Kaiser-tapered sinc interpolant with that of cubic convolution on the example from Figure 4. The accuracy improvement is clearly visible.

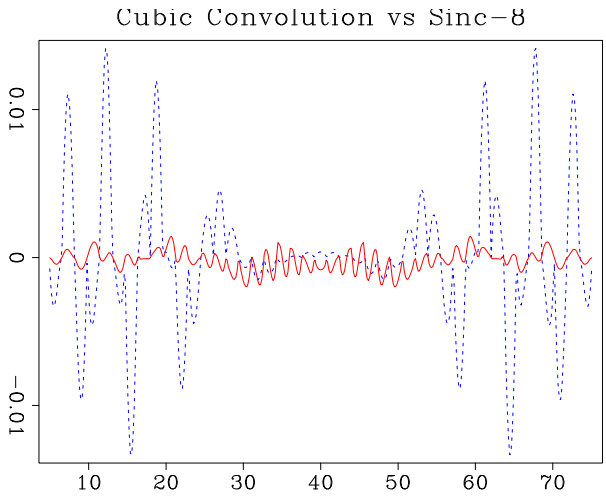

Figure 8: Interpolation error of the cubic-convolution interpolant (dashed line) compared to that of an 8-point windowed sinc interpolant (solid line).

The differences among the described forward interpolation methods are also clearly visible from the discrete spectra of the corresponding interpolants. The left plots in Figures 9 and 10 show discrete interpolation responses: the function $W(x, n)$ for a fixed value of $x = 0.7$. The right plots compare the corresponding discrete spectra. Clearly, the spectrum gets flatter and wider as the accuracy of the method increases.

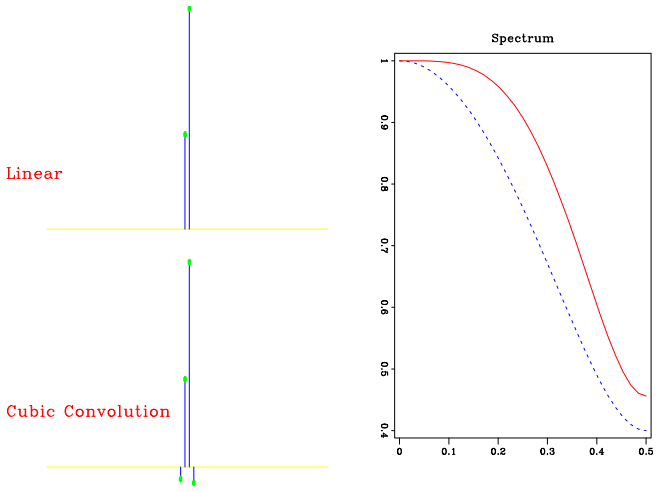

Figure 9: Discrete interpolation responses of linear and cubic convolution interpolants (left) and their discrete spectra (right) for $x = 0.7$.

Discrete Fourier basis

Assuming that the range of the variable x is limited in the interval from $-N$ to N, the discrete Fourier basis (*Fast Fourier Transform*) employs a set of orthonormal

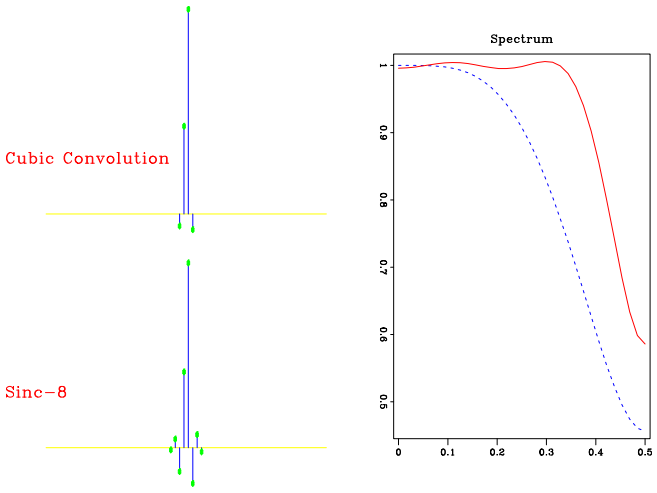

Figure 10: Discrete interpolation responses of cubic convolution and 8-point windowed sinc interpolants (left) and their discrete spectra (right) for $x = 0.7$.

periodic functions

$$\psi_k(x) = \frac{1}{\sqrt{2N}} e^{i\pi \frac{k}{N} x} \;, \tag{23}$$

where the discrete frequency index k also ranges, according to the Nyquist sampling criterion, from $-N$ to N. The interpolation function is computed from equation (15) to be

$$\begin{aligned} W(x,n) &= \frac{1}{2N} \sum_{k=-N}^{N-1} e^{i\pi \frac{k}{N}(x-n)} = \frac{1}{2N} e^{-i\pi(x-n)} \left[1 + e^{i\pi \frac{x-n}{N}} + \cdots + e^{i\pi \frac{2N-1}{N}(x-n)}\right] = \\ &\frac{1}{2N} e^{-i\pi(x-n)} \frac{e^{2i\pi(x-n)} - 1}{e^{i\pi \frac{x-n}{N}} - 1} = \frac{1}{2N} e^{-i\pi \frac{x-n}{2N}} \frac{e^{i\pi(x-n)} - e^{-i\pi(x-n)}}{e^{i\pi \frac{x-n}{2N}} - e^{-i\pi \frac{x-n}{2N}}} = \\ &e^{-i\pi \frac{x-n}{2N}} \frac{\sin\left[\pi(x-n)\right]}{2N \sin\left[\pi(x-n)/2N\right]} \;. \end{aligned} \tag{24}$$

An interpolation function equivalent to (24) has been found by Muir (Lin et al., 1993; Popovici et al., 1993, 1996). It can be considered a tapered version of the sinc interpolant (21) with smooth tapering function

$$\frac{\pi(x-n)/2N}{\tan\left[\pi(x-n)/2N\right]} \;.$$

Unlike most other tapered-sinc interpolants, Muir's interpolant (24) satisfies not only the obvious property (2), but also properties (3) and (19), where the interpolation function $W(x,n)$ should be set to zero for x outside the range from $n-N$ to $n+N$. The form of this function is shown in Figure 11.

The development of the mathematical wavelet theory (Daubechies, 1992) has opened the door to a whole universe of orthonormal function bases, different from the Fourier basis. The wavelet theory should find many useful applications in geophysical data interpolation, but exploring this interesting opportunity would go beyond the scope of the present work.

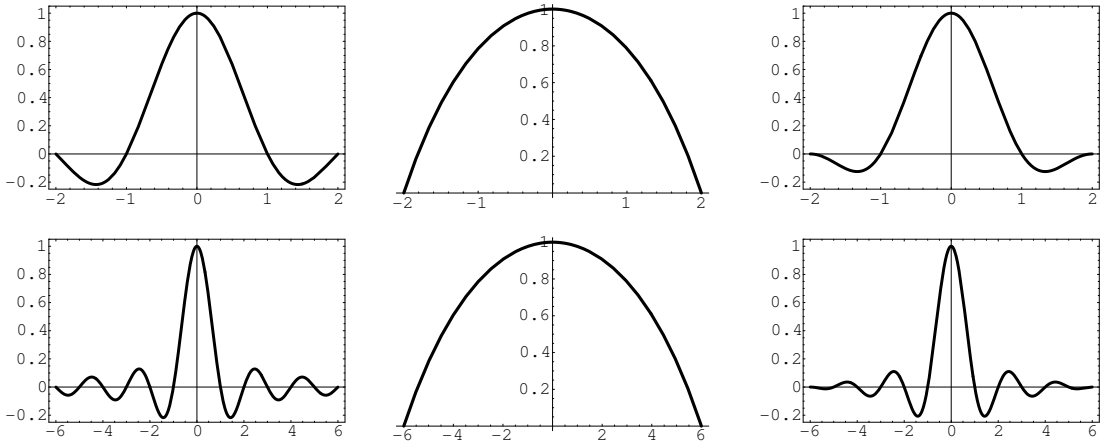

Figure 11: The left plots show the sinc interpolation function. Note the slow decay in x. The middle shows the effective tapering function of Muir's interpolation; the right is Muir's interpolant. The top is for $N = 2$ (5-point interpolation); the bottom, $N = 6$ (13-point interpolation).

The next section carries the analysis to the continuum and compares the mathematical interpolation theory with the theory of seismic imaging.

CONTINUOUS CASE AND SEISMIC IMAGING

Of course, the linear theory is not limited to discrete grids. It is interesting to consider the continuous case because of its connection to the linear integral operators commonly used in seismic imaging. Indeed, in the continuous case, linear decomposition (8) takes the form of the integral operator

$$f(y) = \int m(x) G(y;x) dx \ , \tag{25}$$

where x is a continuous analog of the discrete coefficient k in (8), the continuous function $m(x)$ is analogous to the coefficient c_k, and $G(y;x)$ is analogous to one of the basis functions $\psi_k(x)$. The linear integral operator in (25) has a mathematical form similar to the form of well-known integral imaging operators, such as Kirchhoff migration or "Kirchhoff" DMO. Function $G(y;x)$ in this case represents the Green's function (impulse response) of the imaging operator. Linear decomposition of the data into basis functions means decomposing it into the combination of impulse responses ("hyperbolas").

In the continuous case, equation (15) transforms to

$$W(y,n) = \iint \Psi^{-1}(x_1,x_2) G(y;x_1) \bar{G}(n;x_2) dx_1 \, dx_2 \ , \tag{26}$$

where $\Psi^{-1}(x_1, x_2)$ refers to the inverse of the "matrix" operator

$$\Psi(x_1, x_2) = \int G(y; x_1)\bar{G}(y; x_2)dy \ . \tag{27}$$

When the linear operator, defined by equation (25), is *unitary*,

$$\Psi^{-1}(x_1, x_2) = \delta(x_1 - x_2) \ , \tag{28}$$

and equation (26) simplifies to the single integral

$$W(y, n) = \int G(y; x)\bar{G}(n; x)dx \ . \tag{29}$$

With respect to seismic imaging operators, one can recognize in the interpolation operator (29) the generic form of azimuth moveout (Biondi et al., 1996), which is derived either as a cascade of adjoint ($\bar{G}(n; y)$) and forward ($G(x; y)$) DMO or as a cascade of migration ($\bar{G}(n; y)$) and modeling ($G(x; y)$) (Fomel and Biondi, 1995; Biondi et al., 1998). In the first case, the intermediate variable y corresponds to the space of zero-offset data cube. In the second case, it corresponds to a point in the subsurface.

Asymptotically pseudo-unitary operators as orthonormal bases

It is interesting to note that many integral operators routinely used in seismic data processing have the form of operator (25) with the Green's function

$$G(t, \mathbf{y}; z, \mathbf{x}) = \left|\frac{\partial}{\partial t}\right|^{m/2} A(\mathbf{x}; t, \mathbf{y})\delta\left(z - \theta(\mathbf{x}; t, \mathbf{y})\right) \ . \tag{30}$$

where we have split the variable x into the one-dimensional component z (typically depth or time) and the m-dimensional component $\mathbf{x}$ (typically a lateral coordinate with m equal 1 or 2). Similarly, the variable y is split into t and $\mathbf{y}$. The function θ represents the *summation path*, which captures the kinematic properties of the operator, and A is the amplitude function. In the case of $m = 1$, the fractional derivative $\left|\frac{\partial}{\partial t}\right|^{m/2}$ is defined as the operator with the frequency response $(i\,\omega)^{m/2}$, where ω is the temporal frequency (Samko et al., 1993).

The impulse response (30) is typical for different forms of Kirchhoff migration and datuming as well as for velocity transform, integral offset continuation, DMO, and AMO. Integral operators of that class rarely satisfy the unitarity condition, with the Radon transform (slant stack) being a notable exception. In an earlier paper (Fomel, 1996), I have shown that it is possible to define the amplitude function A for each kinematic path θ so that the operator becomes *asymptotically pseudo-unitary*. This means that the adjoint operator coincides with the inverse in the high-frequency (stationary-phase) approximation. Consequently, equation (28) is satisfied to the same asymptotic order.

Using asymptotically pseudo-unitary operators, we can apply formula (29) to find an explicit analytic form of the interpolation function W, as follows:

$$W(t,\mathbf{y};t_n,\mathbf{y}_n) = \iint G(t,\mathbf{y};z,\mathbf{x})\, G(t_n,\mathbf{y}_n;z,\mathbf{x})\, dz\, d\mathbf{x} =$$

$$\left|\frac{\partial}{\partial t}\right|^{m/2} \left|\frac{\partial}{\partial t_n}\right|^{m/2} \int A(\mathbf{x};t,\mathbf{y})\, A(\mathbf{x};t_n,\mathbf{y}_n)\, \delta\left(\theta(\mathbf{x};t,\mathbf{y}) - \theta(\mathbf{x};t_n,\mathbf{y}_n)\right)\, d\mathbf{x}\ . \tag{31}$$

Here the amplitude function A is defined according to the general theory of asymptotically pseudo-inverse operators as

$$A = \frac{1}{(2\,\pi)^{m/2}}\, \left|F\,\widehat{F}\right|^{1/4}\, \left|\frac{\partial\theta}{\partial t}\right|^{(m+2)/4}\ , \tag{32}$$

where

$$F = \frac{\partial\theta}{\partial t}\,\frac{\partial^2\theta}{\partial\mathbf{x}\,\partial\mathbf{y}} - \frac{\partial\theta}{\partial\mathbf{y}}\,\frac{\partial^2\theta}{\partial\mathbf{x}\,\partial t}\ , \tag{33}$$

$$\widehat{F} = \frac{\partial\widehat{\theta}}{\partial z}\,\frac{\partial^2\widehat{\theta}}{\partial\mathbf{x}\,\partial\mathbf{y}} - \frac{\partial\widehat{\theta}}{\partial\mathbf{x}}\,\frac{\partial^2\widehat{\theta}}{\partial\mathbf{y}\,\partial z}\ , \tag{34}$$

and $\widehat{\theta}(\mathbf{x};t,\mathbf{y})$ is the *dual* summation path, obtained by solving equation $z=\theta(x;t,y)$ for t (assuming that an explicit solution is possible).

For a simple example, let us consider the case of zero-offset time migration with a constant velocity v. The summation path θ in this case is an ellipse

$$\theta(\mathbf{x};t,\mathbf{y}) = \sqrt{t^2 - \frac{(\mathbf{x}-\mathbf{y})^2}{v^2}}\ , \tag{35}$$

and the dual summation path $\widehat{\theta}$ is a hyperbola

$$\widehat{\theta}(\mathbf{y};z,\mathbf{x}) = \sqrt{z^2 + \frac{(\mathbf{x}-\mathbf{y})^2}{v^2}}\ . \tag{36}$$

The corresponding pseudo-unitary amplitude function is found from formula (32) to be (Fomel, 1996)

$$A = \frac{1}{(2\,\pi)^{m/2}}\,\frac{\sqrt{t/z}}{v^m z^{m/2}}\ . \tag{37}$$

Substituting formula (37) into (31), we derive the corresponding interpolation function

$$W(t,\mathbf{y};t_n,\mathbf{y}_n) = \frac{1}{(2\,\pi)^m}\, \left|\frac{\partial}{\partial t}\right|^{m/2} \left|\frac{\partial}{\partial t_n}\right|^{m/2} \int \frac{\sqrt{t\,t_n}}{v^{2m} z^{m+1}}\, \delta(z-z_n)\, d\mathbf{x}\ , \tag{38}$$

where $z=\theta(\mathbf{x};t,\mathbf{y})$, and $z_n=\theta(\mathbf{x};t_n,\mathbf{y}_n)$. For $m=1$ (the two-dimensional case), we can apply the known properties of the delta function to simplify formula (38) further to the form

$$W = \frac{v}{\pi}\, \left|\frac{\partial}{\partial t}\right|^{1/2} \left|\frac{\partial}{\partial t_n}\right|^{1/2} \frac{\sqrt{t\,t_n}}{\sqrt{\left[(\mathbf{y}-\mathbf{y}_n)^2 - v^2(t-t_n)^2\right]\left[v^2(t+t_n)^2 - (\mathbf{y}-\mathbf{y}_n)^2\right]}}\ . \tag{39}$$

The result is an interpolant for zero-offset seismic sections. Like the sinc interpolant in equation (21), which is based on decomposing the signal into sinusoids, equation (39) is based on decomposing the zero-offset section into hyperbolas.

While opening a curious theoretical possibility, seismic imaging interpolants have an undesirable computational complexity. Following the general regularization framework of Chapter **??**, I shift the computational emphasis towards appropriately chosen regularization operators discussed in Chapter **??**. For the forward interpolation method, all data examples in this dissertation use either the simplest nearest neighbor and linear interpolation or a more accurate B-spline method, described in the next section.

INTERPOLATION WITH CONVOLUTIONAL BASES

Unser et al. (1993) noticed that the basis function idea has an especially simple implementation if the basis is convolutional and satisfies the equation

$$\psi_k(x) = \beta(x-k) \ . \tag{40}$$

In other words, the basis is constructed by integer shifts of a single function $\beta(x)$. Substituting expression (40) into equation (8) yields

$$f(x) = \sum_{k \in K} c_k \beta(x-k) \ . \tag{41}$$

Evaluating the function $f(x)$ in equation (41) at an integer value n, we obtain the equation

$$f(n) = \sum_{k \in K} c_k \beta(n-k) \ , \tag{42}$$

which has the exact form of a discrete convolution. The basis function $\beta(x)$, evaluated at integer values, is digitally convolved with the vector of basis coefficients to produce the sampled values of the function $f(x)$. We can invert equation (42) to obtain the coefficients c_k from $f(n)$ by inverse recursive filtering (deconvolution). In the case of a non-causal filter $\beta(n)$, an appropriate spectral factorization will be needed prior to applying the recursive filtering.

According to the convolutional basis idea, forward interpolation becomes a two-step procedure. The first step is the direct inversion of equation (42): the basis coefficients c_k are found by deconvolving the sampled function $f(n)$ with the factorized filter $\beta(n)$. The second step reconstructs the continuous (or arbitrarily sampled) function $f(x)$ according to formula (41). The two steps could be combined into one, but usually it is more convenient to apply them separately. I show a schematic relationship among different variables in Figure 12.

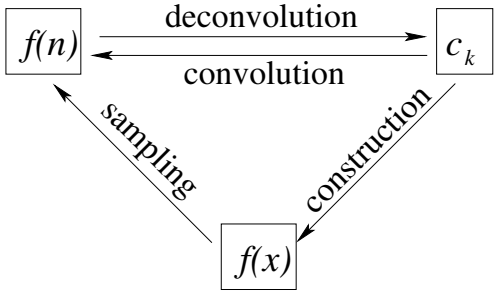

Figure 12: Schematic relationship among different variables for interpolation with a convolutional basis.

B-splines

B-splines represent a particular example of a convolutional basis. Because of their compact support and other attractive numerical properties, B-splines are a good choice of the basis set for the forward interpolation problem and related signal processing problems (Unser, 1999). According to Thévenaz et al. (2000), they exhibit superior performance for any given order of accuracy in comparison with other methods of similar efficiency.

B-splines of the order 0 and 1 coincide with the nearest neighbor and linear interpolants (5) and (6) respectively. B-splines $\beta^n(x)$ of a higher order n can be defined by a repetitive convolution of the zeroth-order spline $\beta^0(x)$ (the box function) with itself:

$$\beta^n(x) = \underbrace{\beta^0(x) * \cdots * \beta^0(x)}_{(n+1) \quad \text{times}} \; . \tag{43}$$

There is also the explicit expression

$$\beta^n(x) = \frac{1}{n!} \sum_{k=0}^{n+1} C_k^{n+1} (-1)^k (x + \frac{n+1}{2} - k)_+^n \; , \tag{44}$$

which can be proved by induction. Here C_k^{n+1} are the binomial coefficients, and the function x_+ is defined as follows:

$$x_+ = \left\{ \begin{array}{ll} x, & \text{for} \quad x > 0 \\ 0, & \text{otherwise} \end{array} \right. \tag{45}$$

As follows from formula (44), the most commonly used cubic B-spline $\beta^3(x)$ has the expression

$$\beta^3(x) = \left\{ \begin{array}{lll} \left(4 - 6|x|^2 + 3|x|^3\right)/6, & \text{for} & 1 > |x| \geq 0 \\ (2 - |x|)^3/6, & \text{for} & 2 > |x| \geq 1 \\ 0, & \text{elsewhere} & \end{array} \right. \tag{46}$$

The corresponding discrete filter $\beta^3(n)$ is a centered 3-point filter with coefficients 1/6, 2/3, and 1/6. According to the traditional method, deconvolution with this filter is performed as a tridiagonal matrix inversion (de Boor, 1978). One can, however,

accomplish the same task more efficiently by spectral factorization and recursive filtering (Unser et al., 1993). The recursive filtering approach generalizes straightforwardly to B-splines of higher orders.

Both the support length and the smoothness of B-splines increase with the order. In the limit, B-splines converge to the Gaussian function. Figures 13 and 14 show the third- and seventh-order splines $\beta^3(x)$ and $\beta^7(x)$, respectively, and their continuous spectra.

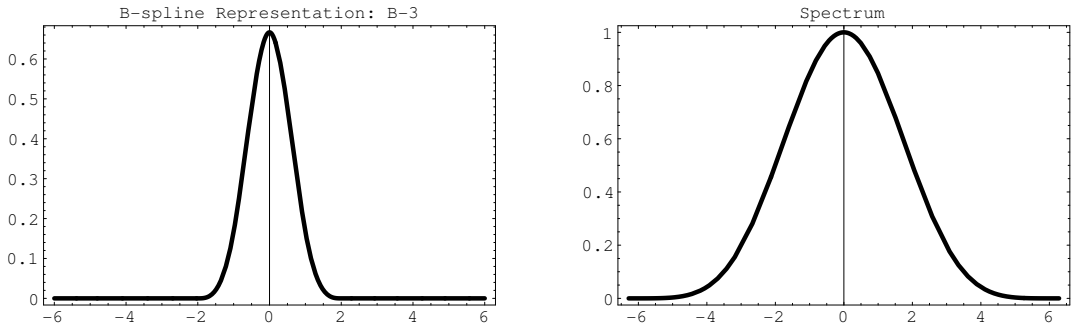

Figure 13: Third-order B-spline $\beta^3(x)$ (left) and its spectrum (right).

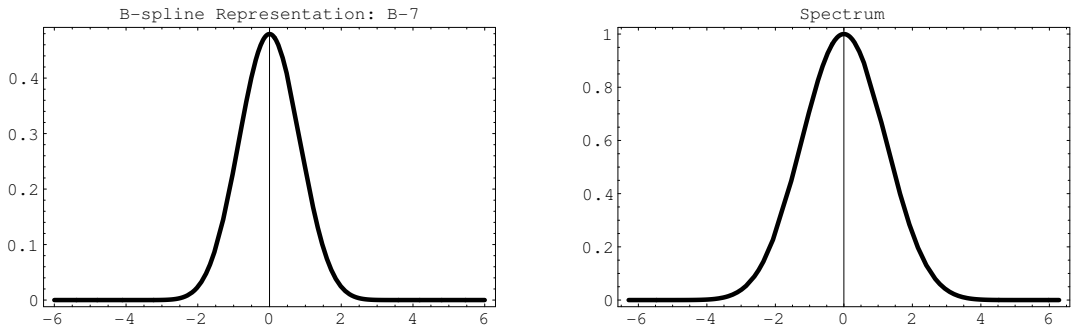

Figure 14: Seventh-order B-spline $\beta^7(x)$ (left) and its spectrum (right).

It is important to realize the difference between B-splines and the corresponding interpolants $W(x, n)$, which are sometimes called *cardinal splines*. An explicit computation of the cardinal splines is impractical, because they have infinitely long support. Typically, they are constructed implicitly by the two-step interpolation method outlined above. The cardinal splines of orders 3 and 7 and their spectra are shown in Figures 15 and 16. As B-splines converge to the Gaussian function, the corresponding interpolants rapidly converge to the sinc function (21). Good convergence is achieved with the help of the implicitly-generated long support, which results from recursive filtering at the first step of the interpolation procedure.

In practice, the recursive filtering step adds only marginally to the total interpolation cost. Therefore, an n-th order B-spline interpolation is comparable in cost with any other method that uses an $(n+1)$-point interpolant. The comparison in accuracy

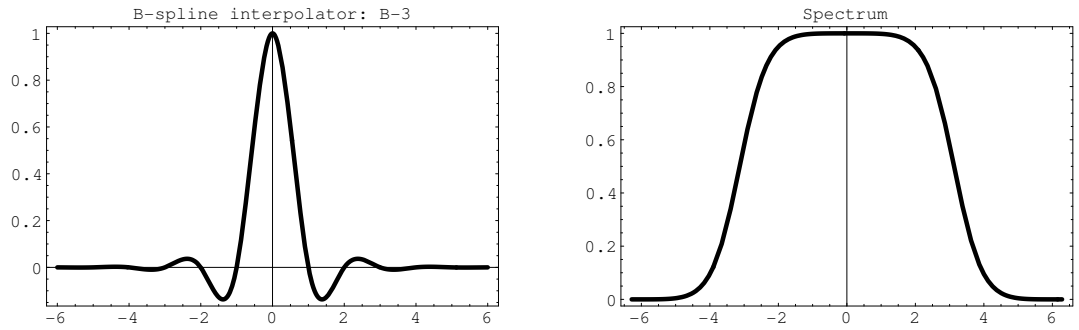

Figure 15: Effective third-order B-spline interpolant (left) and its spectrum (right).

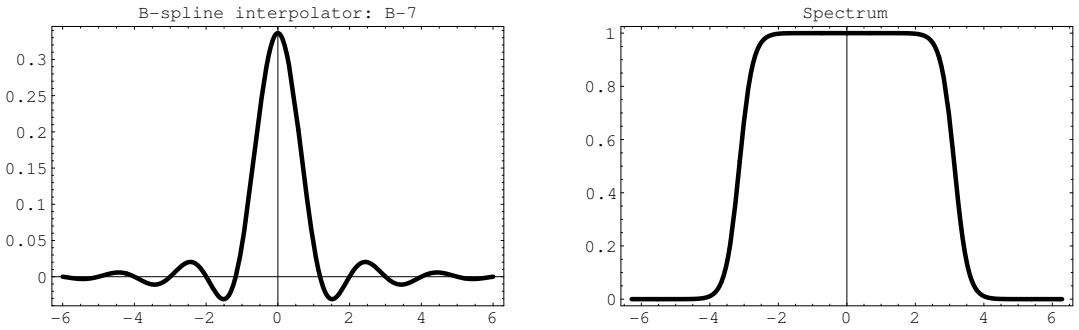

Figure 16: Effective seventh-order B-spline interpolant (left) and its spectrum (right).

usually turns out in favor of B-splines. Figures 17 and 18 compare interpolation errors of B-splines and other similar-cost methods on the example from Figure 4.

Similarly to the comparison in Figures 9 and 10, we can also compare the discrete responses of B-spline interpolation with those of other methods. The right plots in Figures 19 and 20 show that the discrete spectra of the effective B-spline interpolants are genuinely flat at low frequencies and wider than those of the competitive methods. Although the B-spline responses are infinitely long because of the recursive filtering step, they exhibit a fast amplitude decay.

2-D example

For completeness, I include a 2-D forward interpolation example. Figure 21 shows a 2-D analog of the function in Figure 4 and its coarsely-sampled version.

Figure 22 compares the errors of the 2-D nearest neighbor and 2-D linear (bi-linear) interpolation. Switching to bi-linear interpolation shows a significant improvement, but the error level is still relatively high. As shown in Figures 23 and 24, B-spline interpolation again outperforms other methods with comparable cost. In all cases, I constructed 2-D interpolants by orthogonal splitting. Although the splitting method

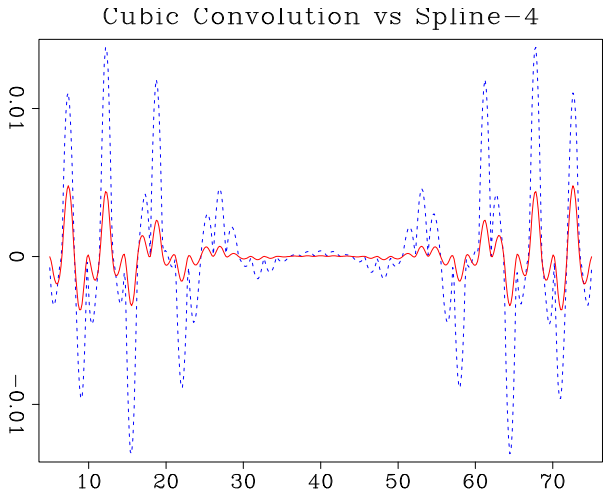

Figure 17: Interpolation error of the cubic-convolution interpolant (dashed line) compared to that of the third-order B-spline (solid line).

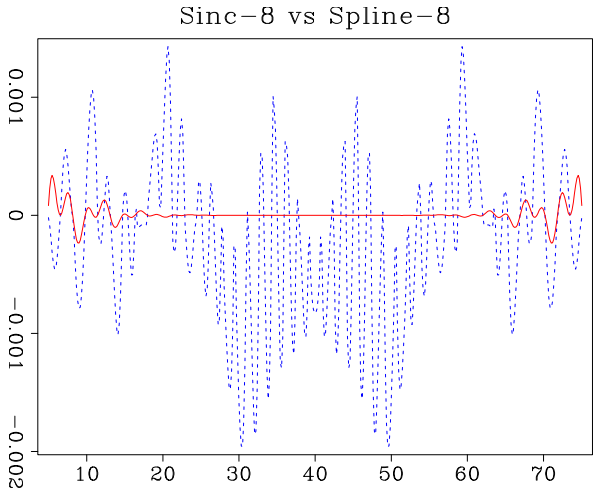

Figure 18: Interpolation error of the 8-point windowed sinc interpolant (dashed line) compared to that of the seventh-order B-spline (solid line).

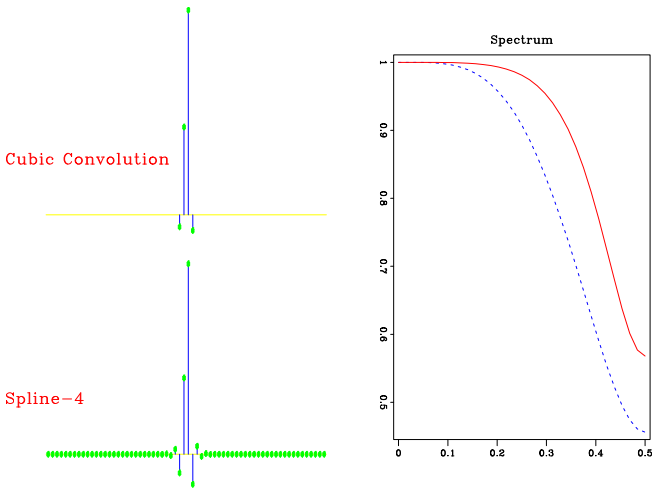

Figure 19: Discrete interpolation responses of cubic convolution and third-order B-spline interpolants (left) and their discrete spectra (right) for $x = 0.7$.

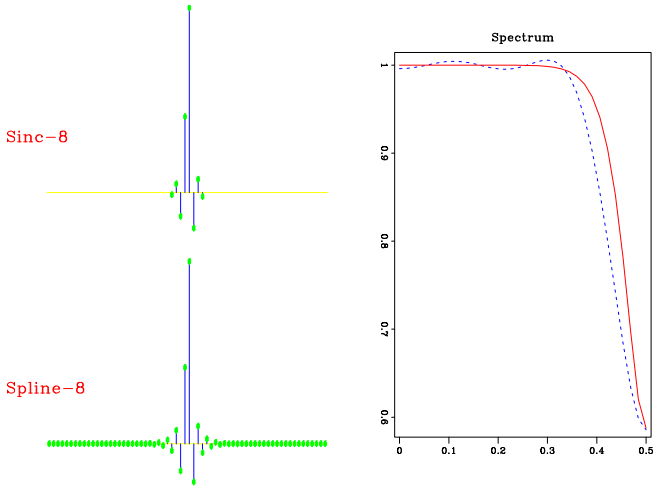

Figure 20: Discrete interpolation responses of 8-point windowed sinc and seventh-order B-spline interpolants (left) and their discrete spectra (right) for $x = 0.7$.

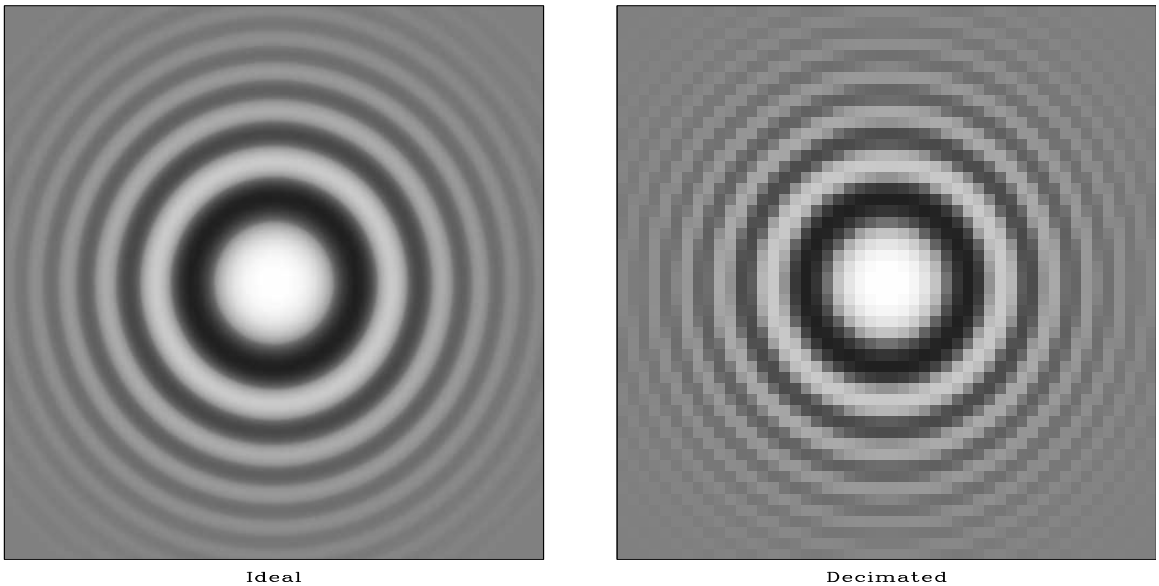

Figure 21: Two-dimensional test function (left) and its coarsely sampled version (right).

reduces computational overhead, the main cost factor is the total interpolant size, which is squared when the interpolation goes from one to two dimensions.

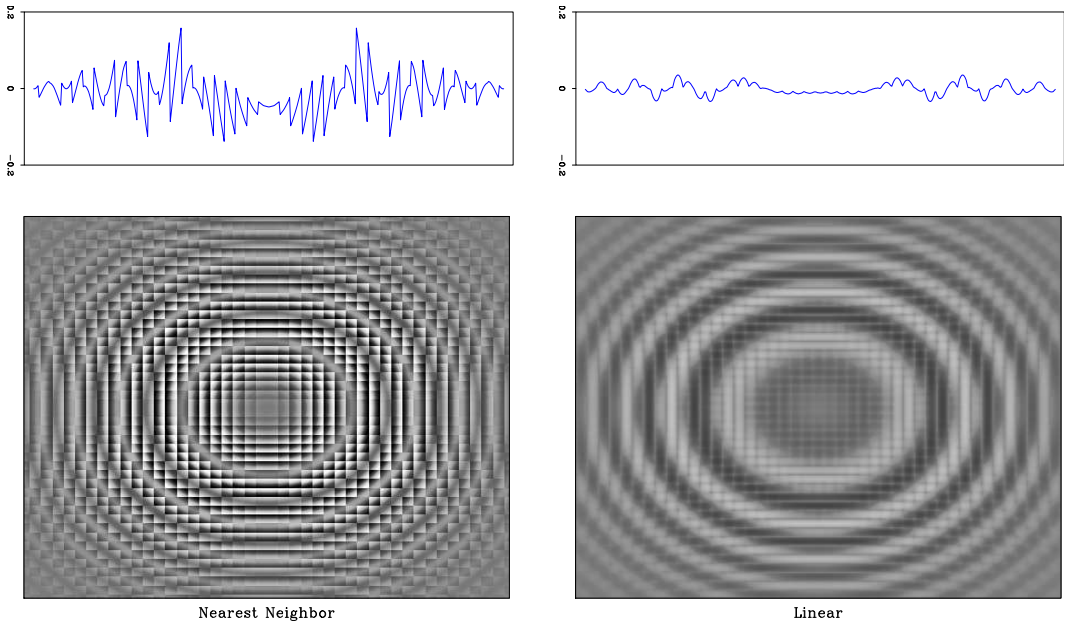

Figure 22: 2-D Interpolation errors of nearest neighbor interpolation (left) and linear interpolation (right). The top graphs show 1-D slices through the center of the image. Bi-linear interpolation exhibits smaller error and therefore is more accurate.

Beyond B-splines

It is not too difficult to construct a convolutional basis with more accurate interpolation properties than those of B-splines, for example by sacrificing the function smoothness. The following piece-wise cubic function has a lower smoothness than $\beta^3(x)$ in equation (46) but slightly better interpolation behavior:

$$\mu^3(x) = \begin{cases} \left(10 - 13|x|^2 + 6|x|^3\right)/16, & \text{for} \quad 1 > |x| \geq 0 \\ (2 - |x|)^2(5 - 2|x|)/16, & \text{for} \quad 2 > |x| \geq 1 \\ 0, & \text{elsewhere} \end{cases} \tag{47}$$

Blu et al. (1998) have developed a general approach for constructing non-smooth piece-wise functions with optimal interpolation properties. However, the gain in accuracy is often negligible in practice. In the rest of the dissertation, I use the classic and better tested B-spline method.

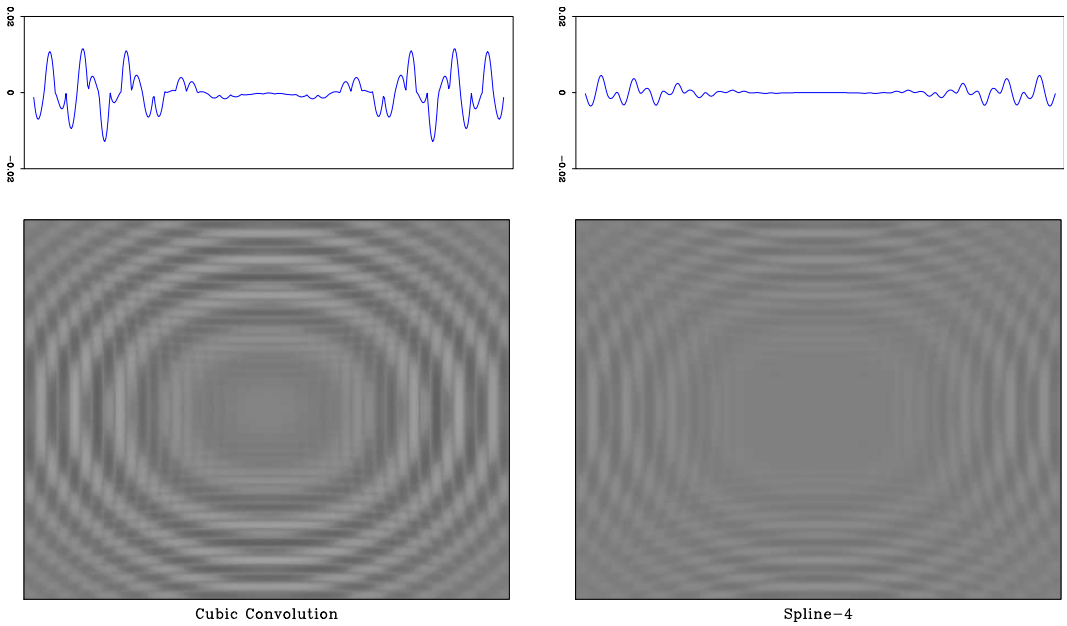

Figure 23: 2-D Interpolation errors of cubic convolution interpolation (left) and third-order B-spline interpolation (right). The top graphs show 1-D slices through the center of the image. B-spline interpolation exhibits smaller error and therefore is more accurate.

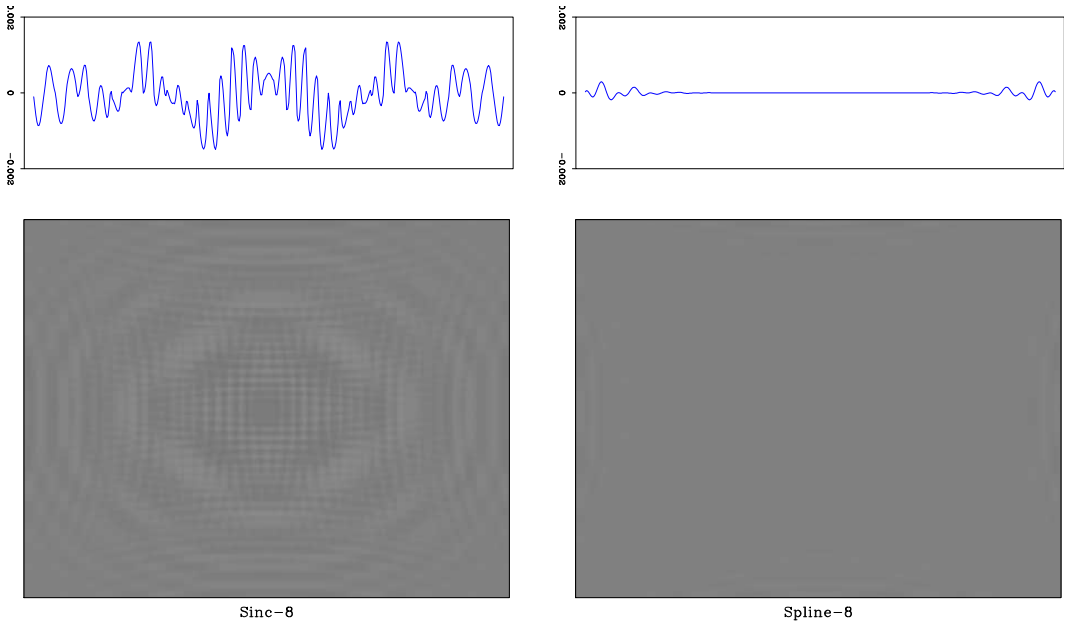

Figure 24: 2-D Interpolation errors of 8-point windowed sinc interpolation (left) and seventh-order B-spline interpolation (right). The top graphs show 1-D slices through the center of the images. B-spline interpolation exhibits smaller error and therefore is more accurate.

SEISMIC APPLICATIONS OF FORWARD INTERPOLATION

For completeness, I conclude this section with two simple examples of forward interpolation in seismic data processing. Figure 25 shows a 3-D impulse response of Stolt migration (Stolt, 1978), computed by using 2-point linear interpolation and 8-point B-spline interpolation. As noted by Ronen (1982) and Harlan (1982), inaccurate interpolation may lead to spurious artifact events in Stolt-migrated images. Indeed, we see several artifacts in the image with linear interpolation (the left plots in Figure 25). The artifacts are removed if we use a more accurate interpolation method (the right plots in Figure 25).

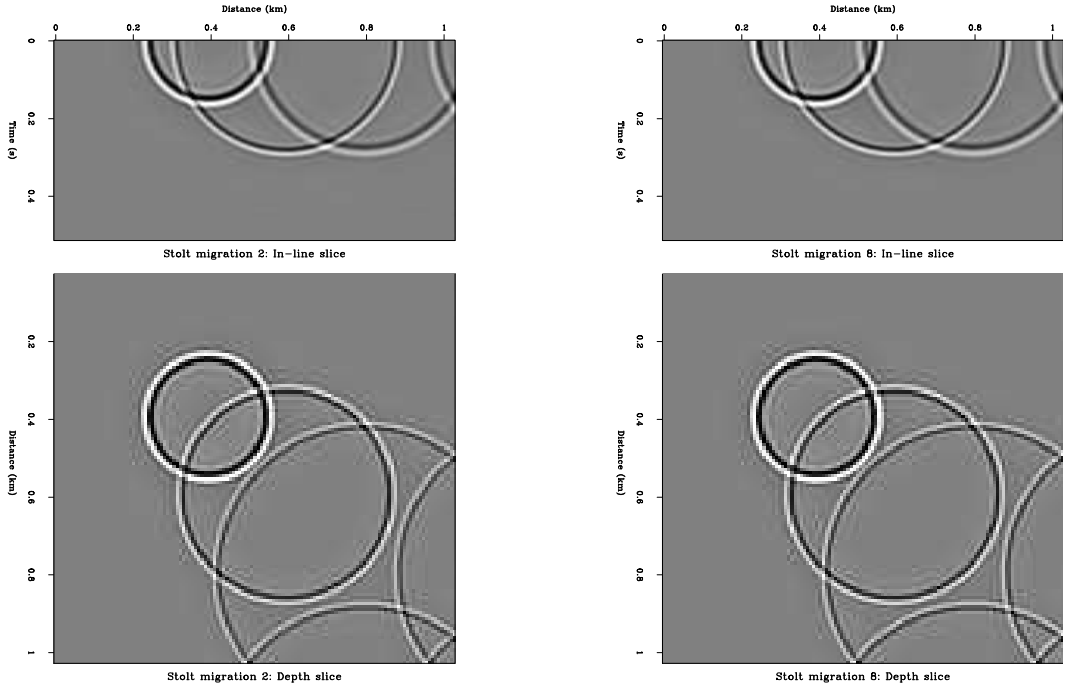

Figure 25: Stolt-migration impulse response. Left: using linear interpolation. Right: using seventh-order B-spline interpolation. Migration artifacts are removed by a more accurate forward interpolation method.

Another simple example is the radial trace transform (Ottolini, 1982). Figure 26 shows a land shot gather contaminated by nearly radial ground-roll. As discussed by Claerbout (1983), Henley (1999, 2000), and Brown and Claerbout (2000a,b), one can effectively eliminate ground-roll noise by applying a radial trace transform followed by high-pass filtering and the inverse radial transform. Figure 27 shows the result of the forward radial transform of the shot gather in Figure 26 in the radial band of the ground-roll noise and the transform error after we go back to the original domain. Comparing the results of using linear and third-order B-spline interpolation, we see once again that the transform artifacts are removed with a more accurate interpolation scheme.

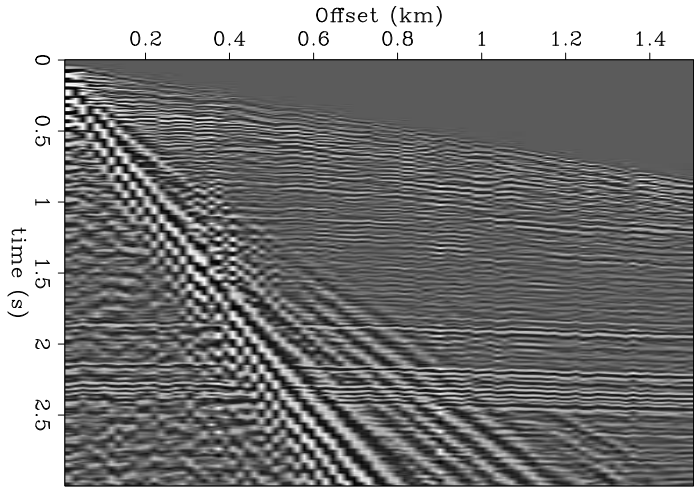

Figure 26: Ground-roll-contaminated shot gather used in a radial transform test

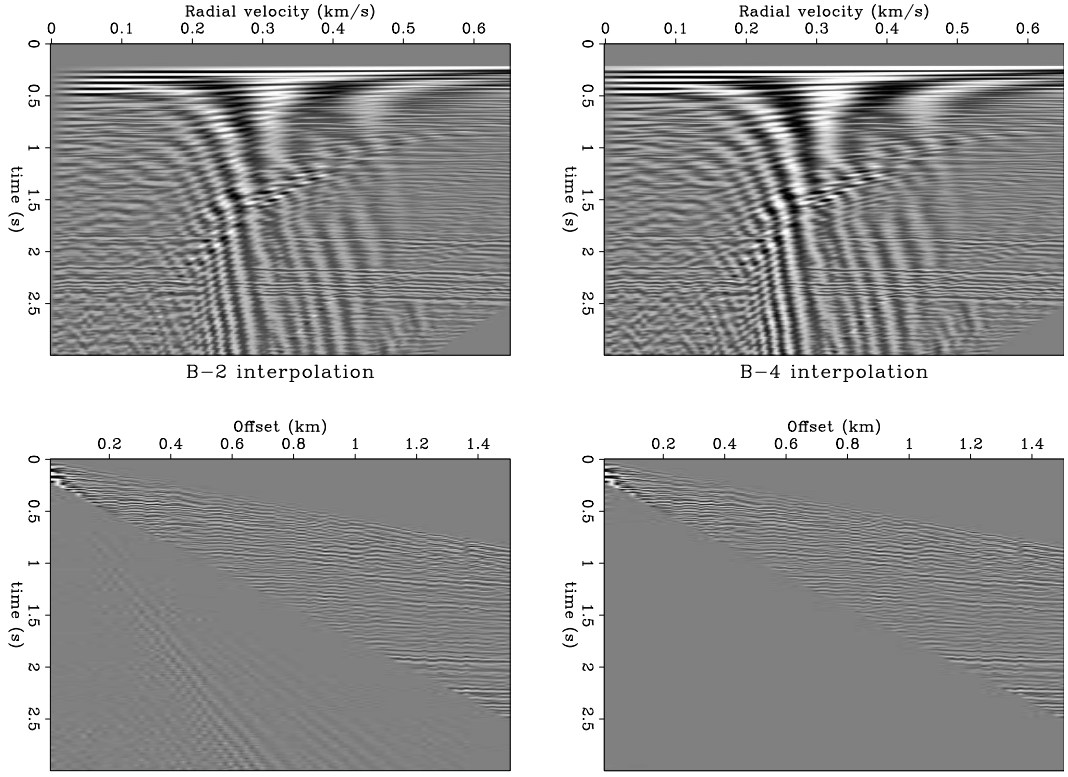

Figure 27: Radial trace transform results. Top: radial trace domain. Bottom: residual error after the inverse transform. The error should be zero in a radial band from 0 to 0.65 km/s radial velocity. Left: using linear interpolation. Right: using third-order B-spline interpolation.

ACKNOWLEDGMENTS

A short conversation with Dave Hale led me to a better understanding of different forward interpolation methods. Tamas Nemeth helped me better understand the general interpolation theory.

REFERENCES

Biondi, B., Fomel, S., and Chemingui, N., 1996, Azimuth moveout for 3-D prestack imaging *in* SEP-93. Stanford Exploration Project, 15–44.

—, 1998, Azimuth moveout for 3-D prestack imaging: Geophysics, **63**, 574–588.

Blu, T., Thévenaz, P., and Unser, M., 1998, Minimum support interpolators with optimum approximation properties *in* Proc. IEEE Int. Conf. Image Processing, Chicago, IL, USA, October 4 -7. IEEE, 242–245.

de Boor, C., 1978, A practical guide to splines: Springer-Verlag.

Brown, M., and Claerbout, J., 2000a, Ground roll and the Radial Trace Transform - revisited *in* SEP-103. Stanford Exploration Project, 219–237.

—, 2000b, A pseudo-unitary implementation of the radial trace transform *in* 70th Ann. Internat. Mtg. Soc. of Expl. Geophys., 2115–2118.

Claerbout, J. F., 1983, Ground roll and radial traces *in* SEP-35. Stanford Exploration Project, 43–54.

—, 1992, Earth Soundings Analysis: Processing Versus Inversion: Blackwell Scientific Publications.

Daubechies, I., 1992, Ten lectures on wavelets: SIAM, Philadelphia, Pennsylvania.

Fomel, S., 1996, Stacking operators: Adjoint versus asymptotic inverse *in* SEP-92. Stanford Exploration Project, 267–292.

Fomel, S., and Biondi, B., 1995, The time and space formulation of azimuth moveout *in* SEP-84. Stanford Exploration Project, 25–38.

Garcia, A. G., 2000, Orthogonal sampling formulas: A unified approach: SIAM Review, **42**, 499–512.

Hale, I. D., 1980, Resampling irregularly sampled data *in* SEP-25. Stanford Exploration Project, 39–58.

Harlan, W. S., 1982, Avoiding interpolation artifacts in Stolt migration *in* SEP-30. Stanford Exploration Project, 103–110.

Henley, D., 1999, The radial trace transform: An effective domain for coherent noise attenuation and wavefield separation *in* 69th Ann. Internat. Mtg. Soc. of Expl. Geophys., 1204–1207.

—, 2000, Wavefield separation and other useful applications in the radial trace domain *in* 70th Ann. Internat. Mtg. Soc. of Expl. Geophys., 2111–2114.

Kaiser, J. F., and Shafer, R. W., 1980, On the use of the I0-Sinh window for spectrum analysis: IEEE Trans. Acoustics, Speech and Signal Processing, **ASSP-28(1)**, 105.

Karrenbach, M., 1995, Elastic tensor wave fields: Ph.D. thesis, Stanford University.

Keys, R. G., 1981, Cubic convolution interpolation for digital image processing: IEEE Trans. Acoust., Speech, Signal Process., **ASSP-29**, 1153–1160.

Kotel'nikov, V. A., 1933, On the transmission capacity of "ether" and wire in electr ocommunications: Izd. Red. Upr. Svyazi RKKA.

Lin, J., Teng, L., and Muir, F., 1993, Comparison of different interpolation methods for Stolt migration *in* SEP-79. Stanford Exploration Project, 255–260.

Ottolini, R., 1982, Migration of reflection seismic data in angle-midpoint coordinates: Ph.D. thesis, Stanford University.

Popovici, A. M., Blondel, P., and Muir, F., 1993, Interpolation in Stolt migration *in* SEP-79. Stanford Exploration Project, 261–264.

Popovici, A. M., Muir, F., and Blondel, P., 1996, Stolt redux: A new interpolation method: Journal of Seismic Exploration, **5**, 341–347.

Ronen, J., 1982, Stolt migration; interpolation artifacts *in* SEP-30. Stanford Exploration Project, 95–102.

Samko, S. G., Kilbas, A. A., and Marichev, O. I., 1993, Fractional integrals and derivatives: theory and application s: Gordon and Breach Science Publishers.

Shannon, C. E., 1949, Communication in the presense of noise: Proc. I.R.E., **37**, 10–21.

Stolt, R. H., 1978, Migration by Fourier transform: Geophysics, **43**, 23–48.

Thévenaz, P., Blu, T., and ser, M. U., 2000, Image interpolation and resampling *in* Handbook of Medical Imaging, Processing and Analysis. Academic Press, 393–420.

Unser, M., 1999, Splines: a perfect fit for signal and image processing: IEEE Signal Processing Magazine, **16**, 22–38.

Unser, M., Aldroubi, A., and Eden, M., 1993, B-spline signal processing: Part I – Theory: IEEE Transactions on Signal Processing, **41**, 821–832.

Wolberg, G., 1990, Digital image warping: IEEE Computer Society Press.